AIP Advances

Numerical study of dispersion of nanoparticles in magnetohydrodynamic liquid with Hall and ion slip currents

Cite as: AIP Advances **9**, 025219 (2019); https://doi.org/10.1063/1.5084311
Submitted: 06 December 2018 • Accepted: 13 February 2019 • Published Online: 26 February 2019

Imran Haider Qureshi, M. Nawaz and A. Shahzad

Numerical study of dispersion of nanoparticles in magnetohydrodynamic liquid with Hall and ion slip currents

Cite as: AIP Advances 9, 025219 (2019); doi: 10.1063/1.5084311
Submitted: 6 December 2018 • Accepted: 13 February 2019 •
Published Online: 26 February 2019

Imran Haider Qureshi,[1,a)] M. Nawaz,[1] and A. Shahzad[2]

AFFILIATIONS

[1] Department of Applied Mathematics & Statistics, Institute of Space Technology, Islamabad 44000, Pakistan
[2] Department of Aeronautics & Astronautics, Institute of Space Technology, Islamabad 44000, Pakistan

[a)] Email: imran_haider707@yahoo.com (Imran Haider Qureshi)

ABSTRACT

Heat transfer in partially ionized Erying-Powell liquid containing four types of nano-particles is discussed in this manuscript. Mathematical models for the mixture Erying-Powell plasma and nano-particles are developed and are solved by using finite element method (FEM). Numerical computations are carried out under tolerance 10^{-5}. Physical parameters have significant effects on both thermal boundary layer thicknesses and momentum boundary layer thicknesses. Shear stresses at the surface can be minimized by the Hall and ion slip currents whereas the shear stresses at the sheet for Erying-Powell fluid are high as comparing to the Newtonian fluid. The rate of transfer of heat is significantly influenced by Hall and ion slip parameters. Highest rate of transfer of heat is observed for the case of TiO_2 nano-particles. Therefore, it is recommended to disperse TiO_2 nano-particles in Erying-Powell fluid for enhancement of heat transfer in Erying-Powell plasma.

I. INTRODUCTION

Blood and other biological fluids are those which do not follow Newton's law of viscosity and are called non-Newtonian fluids. Newtonian and non-Newtonian fluids flows play an important role in engineering processes. For example, fiber making, plastic manufacturing, metal spinning, tooth pastes, yogurt, clay coating, physiological liquids (bile, synovial fluid, blood), petroleum products, lubricants etc. Erying-Powell fluid is non-Newtonian fluid and its constitutive equations are reducible to the constitutive equations of Newtonian at high and low shear rate.[1] Several investigators have explored the flow of Erying-Powell fluid in different scenarios. Here we will describe some latest studies on the flow of Erying-Powell fluid. For example, Nadeem and Saleem[2] considered transport of mass and heat in Erying-Powell fluid over a rotating cone. Hayat et al.[3] studied the effects of magnetic fluid on heat transfer in radiative three-dimensional flow of Erying-Powell fluid over a moving surface. Khader and Megahed[4] analyzed the effects of transfer of heat in unsteady thin film flow of Erying-Powell fluid. Jalil and Asghar[5] discussed heat transfer characteristics in the flow of Erying-Powell fluid. Elbade et al.[6] considered the combined effects of viscous dissipation and magnetic field in Erying-Powell fluid in the porous medium. Finite element study of heat transfer in Erying-Powell fluid was performed by Poonia et al.[7] The effect of melting phenomenon of sheet on the transfer of heat in Erying-Powell fluid is discussed by Hayat et al.[8] Javed et al.[9] considered the flow of Erying-Powell fluid over a stretching surface. The effect of thermophoretic and chemical reaction on the transport of mass and heat in Erying-Powell fluid are studied by Khan et al.[10] Ashraf et al.[11] considered three dimensional heat transfer in nano-Erying-Powell fluid over an exponentially stretching. The Erying-Powell rheology is characterized by the following tensor[1–11]

$$\tau_{ij} = \mu \frac{\partial u_i}{\partial x_j} + \frac{1}{\beta}\sinh^{-1}\left(\frac{1}{c}\frac{\partial u_i}{\partial x_j}\right), \text{ with } \sinh^{-1}\left(\frac{1}{c}\frac{\partial u_i}{\partial x_j}\right) = \frac{1}{c}\frac{\partial u_i}{\partial x_j} - \frac{1}{6}\left(\frac{1}{c}\frac{\partial u_i}{\partial x_j}\right)^3, \tag{1}$$

TABLE I. Physical properties of nanoparticles and blood.[35]

Physical property	blood	Cu	Ag	Al_2O_3	TiO_2
$\rho/(m^{-3}Kg)$	1060	8933	10500	3970	4250
$c_p/(K^{-1}Jkg^{-1})$	3770	385	235	765	686.2
$k/(K^{-1}Wm^{-1})$	0.492	401	429	40	8.9538
ϕ	0.00	0.05	0.10	0.15	0.20
$\sigma/(s.m^{-1})$	4.3×10^{-5}	59.6×10^{6}	6.6×10^{-7}	35×10^{6}	2.6×10^{6}

where c and β are material fluid parameters and μ is dynamics viscosity. The constitutive relation (1) reduces to the Newtonian case when $c \to \infty$.

Transport of heat and mass is of great interest for the mathematicians as well as engineers. Various theoretical studies on transport of heat and mass are published. For instance, Ashraf et al.,[12] analytically analyzed the transport of heat in the flow of viscoelastic fluid over an exponentially stretching surface. Awais et al.[13] studied steady flow of Burger's liquid in the presence of melting heat phenomenon. Ramesh et al.[14] computed numerical solutions of problems governing MHD dusty fluid in the presence of heat generation. Ramzan et al.[15] reconnoitered MHD Maxwell fluid flow over a bidirectional stretching surface and discussed the impact of physical parameters. Majeed et al.[16] considered the influence of chemical reaction on the flow of Ferro-fluid exposed to magnetic dipoles and resulting problem is solved by the shooting scheme.

Flow of partially ionized fluid exposed to magnetic field can be modeled using following generalized Ohm's law[18–28]

$$\mathbf{J} + \frac{\omega_e\tau_e}{B_\circ}\mathbf{J}\times\mathbf{B} - \frac{\omega_e\tau_e\omega_i\tau_i}{B_\circ^2}(\mathbf{J}\times\mathbf{B})\times\mathbf{B} = \sigma[\mathbf{E}+\mathbf{V}\times\mathbf{B}], \tag{2}$$

with usual conservation law and set of Maxwell's equations.

In Eq. (2), $\mathbf{J}$ is current density, $\mathbf{B}$ is magnetic induction, σ is electrical conductivity, ω_i is ion collision frequency, ω_e is electron collision frequency, τ_e is electron collision time, τ_i is ion collision time and $B_\circ$ is magnitude of the magnetic induction.

The emission of thermal radiation in the form of electromagnetic waves during transfer of heat has a great impact on the flow characteristics and it established fact that the thermal radiations are electromagnetic waves which carry heat energy away from the fluid regime. The amount of heat emitted per unit volume in the form of thermal radiations can be calculated through Stefan Boltzmann law. This law states that radiative heat flux vector is directly proportional to the fourth power of temperature minus fourth power of the ambient temperature.

$$\mathbf{q}_r = -\frac{4\sigma^*}{3k^*}\nabla(T^4 - T_\infty^4), \tag{3}$$

where T is the temperature of fluid, k^* is the Rosseland mean absorption coefficient, σ^* is the Stefan Boltzmann constant and T_∞ is the ambient temperature. The Stefan Boltzmann law given in Eq. (3) has been used by many researchers.[29–31] The rate of radiative heat away per unit volume is

$$\frac{dQ_r}{dt} = -\nabla\cdot\mathbf{q}_r = \frac{16\sigma^* T_\infty^3}{3k^*}\nabla^2 T. \tag{4}$$

A. Relationship between thermo-physical properties of base fluid and nano-particles

There are various models (empirical formulas) describing the relationship between thermophysical properties of the base fluid, metallic nano-particles and nanofluid but here in this study, we have followed Das et al.[17] The model used by Das et al.[17] is

$$\rho_{nf} = \phi\rho_s + (1-\phi)\rho_f, (\rho c_p)_{nf} = \phi(\rho c_p)_s + (1-\phi)(\rho c_p)_f,$$

$$\mu_{nf} = \frac{\mu_f}{(1-\phi)^{2.5}},$$

$$\sigma_{nf} = \sigma_f\left(1 + \frac{3(\sigma-1)\phi}{\sigma+2-(\sigma-1)\phi}\right), \quad \sigma = \frac{\sigma_s}{\sigma_f},$$

$$k_{nf} = \frac{k_s + 2k_f - 2\phi(k_f - k_s)}{k_s + 2k_f + \phi(k_f - k_s)}k_f,$$

where k, ρ, σ, ϕ and c_p, respectively, are the density, the thermal conductivity, the electrical conductivity, the volume fraction and the specific heat. The subscripts nf, f and s stand for nanofluid, fluid and solid particles (nano-particles) respectively. Thermo-physical properties of four types of metallic nano-particles and blood are described in Table I.

To the best of our knowledge, no study considering the effect of Hall and ion slip currents on three-dimensional heat transfer in partially ionized Erying-Powell liquid is discussed yet. The present work fills this gape. This study is organized in five sections. Flow situation and its modeling is given in Section II. Computational procedure is discussed in Section III. The results are discussed in Section IV. Results are briefly discussed in Section V.

II. PHYSICAL SITUATION AND MATHEMATICAL MODELING

Let us consider the enhancement of heat transfer in a partially ionized non-Newtonian fluid (Eyring-Powell) over an elastic sheet moving with velocity $\boldsymbol{V_w} = U_w\boldsymbol{i} + V_w\boldsymbol{j} = a(x+y)^{\frac{1}{3}}\boldsymbol{i} + b(x+y)^{\frac{1}{3}}\boldsymbol{j}$. Here a and b are constants having units $m^{\frac{2}{3}}/s$. A non-uniform magnetic field $B_\circ(x+y)^{-\frac{1}{3}}\boldsymbol{k}$ is applied along z-axis, perpendicular to the sheet. The fluid over sheet is subjected to the dispersion of four types of nano-particles (Cu, Ag, Al_2O_3 and TiO_2). The sheet is maintained at non-uniform temperature $T_w(x,y) = dT_\circ(x+y)^{\frac{2}{3}} + T_\infty$ in which d and $T_\circ$ have units $1/m^{\frac{2}{3}}$ and K (kelvin). Hall and ion currents are of considerable order of magnitudes. The said fluid occupies half space $-\infty < x < \infty$, $-\infty < y < \infty$ and $0 < z < \infty$. The schematic representation is given by Fig. 1.

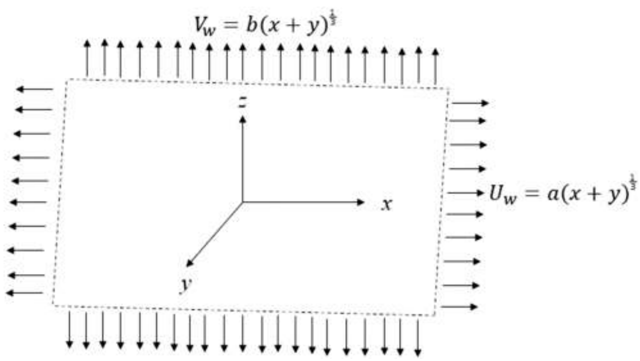

FIG. 1. Physical model and coordinate system.

The conservation laws and generalized Ohm's law under the boundary layer approximations take the following form

$$\frac{\partial u}{\partial x} + \frac{\partial v}{\partial y} + \frac{\partial w}{\partial z} = 0 \tag{5}$$

$$u\frac{\partial u}{\partial x} + v\frac{\partial u}{\partial y} + w\frac{\partial u}{\partial z} = (\upsilon_{nf} + \frac{1}{\beta c \rho_{nf}})\frac{\partial^2 u}{\partial z^2} - \frac{1}{2\beta c^3 \rho_{nf}}(\frac{\partial u}{\partial z})^2 \frac{\partial^2 u}{\partial z^2} + \frac{\sigma_{nf}\, B_\circ^2 (x+y)^{-\frac{2}{3}}}{\rho_{nf}\,[\beta_e^2 + (1+\beta_e\beta_i)^2]} \times [\beta_e v - (1+\beta_e\beta_i)u], \tag{6}$$

$$u\frac{\partial v}{\partial x} + v\frac{\partial v}{\partial y} + w\frac{\partial v}{\partial z} = (\upsilon_{nf} + \frac{1}{\beta c \rho_{nf}})\frac{\partial^2 v}{\partial z^2} - \frac{1}{2\beta c^3 \rho_{nf}}(\frac{\partial v}{\partial z})^2 \frac{\partial^2 v}{\partial z^2} - \frac{\sigma_{nf}\, B_\circ^2 (x+y)^{-\frac{2}{3}}}{\rho_{nf}\,[\beta_e^2 + (1+\beta_e\beta_i)^2]}[\beta_e u + (1+\beta_e\beta_i)v], \tag{7}$$

$$u\frac{\partial T}{\partial x} + v\frac{\partial T}{\partial y} + w\frac{\partial T}{\partial z} = (\frac{k_{nf}}{(\rho c_p)_{nf}} + \frac{16\sigma^* T_\infty^3}{3(\rho c_p)_{nf}\, k^*})\frac{\partial^2 T}{\partial z^2} + \frac{\sigma_{nf}\, B_\circ^2 (x+y)^{-\frac{2}{3}}}{(\rho c_p)_{nf}\,[\beta_e^2 + (1+\beta_e\beta_i)^2]}[u^2 + v^2], \tag{8}$$

where υ is the kinematics viscosity.

Following boundary conditions will be implemented for the solutions of the flow equations

$$\left.\begin{aligned} u(x,y,0) = U_w,\ v(x,y,0) = V_w,\ w(x,y,0) = 0,\ T(x,y,0) = T_w, \\ u \to 0,\ v \to 0,\ T \to T_\infty, \quad \text{as} \quad z \to \infty. \end{aligned}\right\} \tag{9}$$

Equations (5)–(9) can be normalized by the following transformation

$$\begin{gathered} u = a(x+y)^{\frac{1}{3}} f', \quad v = a(x+y)^{\frac{1}{3}} g', \\ w = -\sqrt{a\upsilon_f}\,(x+y)^{-\frac{1}{3}}(\frac{2}{3}(f+g) - \frac{1}{3}\eta(f'+g')), \\ \theta = \frac{T - T_\infty}{T_w - T_\infty}, \quad \eta = \sqrt{\frac{a}{\upsilon_f}}(x+y)^{-\frac{1}{3}} z, \end{gathered} \tag{10}$$

and, hence, one obtains

$$\left.\begin{gathered} (1+\varepsilon(1-\phi)^{2.5})f''' - \phi_1[\tfrac{1}{3}(g'+f')f' - \tfrac{2}{3}(f+g)f''] \\ -\varepsilon(1-\phi)^{2.5}\delta(f'')^2 f''' + \phi_2 \tfrac{M^2}{\beta_e^2+(1+\beta_e\beta_i)^2}[\beta_e g' - (1+\beta_e\beta_i)f'] = 0 \\ f\ (0) = 0, f'(0) = 1, f'(\infty) = 0, \end{gathered}\right\} \tag{11}$$

$$\left.\begin{gathered} (1+\varepsilon(1-\phi)^{2.5})g''' - \phi_1[\tfrac{1}{3}(f'+g')g' - \tfrac{2}{3}(f+g)g''] \\ -\varepsilon(1-\phi)^{2.5}\delta(g'')^2 g''' - \phi_2 \tfrac{M^2}{\beta_e^2+(1+\beta_e\beta_i)^2}[\beta_e f' + (1+\beta_e\beta_i)g'] = 0 \\ g(0) = 0, g'(0) = \lambda, g'(\infty) = 0, \end{gathered}\right\} \tag{12}$$

$$\left.\begin{gathered} (1+\tfrac{4}{3N_r})\theta'' + \tfrac{2k_f}{3k_{nf}}\phi_3 \Pr(f+g)\theta' - \frac{2}{3}\tfrac{k_f}{k_{nf}}\phi_3 \Pr(f'+g')\theta \\ + \tfrac{k_f}{k_{nf}}\tfrac{\phi_2}{(1-\phi)^{2.5}}\tfrac{M^2 Ec \Pr}{\beta_e^2+(1+\beta_e\beta_i)^2}[f'^2 + g'^2] = 0, \\ \theta(0) = 1, \theta(\infty) = 0, \end{gathered}\right\} \tag{13}$$

where

$$\begin{gathered} \phi_1 = (1-\phi)^{\frac{5}{2}}(1-\phi+\phi\tfrac{\rho_s}{\rho_f}), \quad \phi_2 = (1-\phi)^{\frac{5}{2}}(1+\tfrac{3(\sigma-1)\phi}{\sigma+2-(\sigma-1)\phi}), \\ \phi_3 = 1-\phi+\tfrac{\phi(\rho c_p)_s}{(\rho c_p)_f} \end{gathered} \tag{14}$$

with ε and δ are the fluid parameters, M is the magnetic parameter, Pr is the Prandtl number, Ec is the Eckert number, N_r is the radiation parameter, λ is the stretching ratio parameter, β_e and β_i is the Hall and ion slip parameters. These parameters are expressed as

$$\begin{gathered} \varepsilon = \frac{1}{\mu_{nf}\beta c}, \delta = \frac{a^3}{2\upsilon_f c}, M^2 = \frac{\sigma_f B_\circ^2}{\rho_f a}, \Pr = \frac{\mu_f (c_p)_f}{k_f}, Ec = \frac{a^2}{(c_p)_f\, dT_\circ}, \\ N_r = \frac{k_{nf} k^*}{4\sigma^* T_\infty^3}, \lambda = \frac{b}{a}, \beta_e = \omega_e\tau_e, \beta_i = \omega_i\tau_i. \end{gathered}$$

The velocity and temperature gradients in normalized forms are

$$\begin{aligned} C_{f_x} &= \frac{\tau_{zx}|_{z=0}}{\rho_f a^2 (x+y)^2} = \frac{1}{\rho_f a^2 (x+y)^2} \times \left((\mu_{nf} + \frac{1}{\beta c})\frac{\partial u}{\partial z} - \frac{\varepsilon}{6\beta c^3}(\frac{\partial u}{\partial z})^3\right)\Bigg|_{z=0} \\ &= \frac{1}{(\mathrm{Re})^{\frac{1}{2}}}\left((1+\varepsilon)(1-\phi)^{-2.5} f''(0) - \frac{\varepsilon}{3}\delta(f''(0))^3\right), \end{aligned} \tag{15}$$

$$\begin{aligned} C_{g_y} &= \frac{\tau_{zy}|_{z=0}}{\rho_f\, a^2 (x+y)^2} = \frac{1}{\rho_f\, a^2 (x+y)^2} \times \left((\mu_{nf} + \frac{1}{\beta c})\frac{\partial v}{\partial z} - \frac{\varepsilon}{6\beta c^3}(\frac{\partial v}{\partial z})^3\right)\Bigg|_{z=0} \\ &= \frac{1}{(\mathrm{Re})^{\frac{1}{2}}}\left((1+\varepsilon)(1-\phi)^{-2.5} g''(0) - \frac{\varepsilon}{3}\delta(g''(0))^3\right), \end{aligned} \tag{16}$$

$$Nu = \frac{-k_{nf}\,(x+y)\frac{\partial T}{\partial z}\big|_{z=0}}{k_f\,(T_w - T_\infty)} = -\frac{k_{nf}}{\mathrm{Re}^{1/2} k_f}\theta'(0), \tag{17}$$

where $\mathrm{Re} = a(x+y)^{\frac{2}{3}}/\upsilon_f$.

III. FINITE ELEMENT FORMULATION: A COMPUTATIONAL PROCEDURE

Galerkin finite element method[32–35] is very strong tool to solve the system of nonlinear differential equations. The detailed procedure of GFEM for this work is given in following steps.

Discretization of domain: Discretization of domain involves the breakdown of domain into smaller domain. In present case the domain is one dimensional and discretized into line segment, two nodes per segments.

Selection of interpolation functions: Field variables are interpolated by using interpolation functions. Interpolation functions are often polynomials. In the case of line elements (two nodes per elements) linear polynomial is used which is given by

$$\psi_j = (-1)^{j-1}\Big(\frac{\eta_{j+1}-\eta}{\eta_{j+1}-\eta_j}\Big), \quad j = 1, 2 \tag{18}$$

Selection of weight functions: Different methods are used for the selection of weight function. In GFEM, interpolation functions are taken as weight functions.

Construction of residuals and weak form: The approximate solution do not satisfy the problems and what we get by substitution of approximate solution in the differential equations is called residual and inner product of weight function and residual in integral sense gives weighted residual integrals and integration of highest order linear term gives the weak form. Hence,

$$\int_{\eta_e}^{\eta_{e+1}} w_i(f' - h)\,d\eta = 0, \tag{19}$$

$$\int_{\eta_e}^{\eta_{e+1}} w_i(g' - R)\,d\eta = 0, \tag{20}$$

$$\begin{aligned}\int_{\eta_e}^{\eta_{e+1}} w_i\Big[&(1+\varepsilon(1-\phi)^{2.5})h'' - \frac{1}{3}\phi_1(h+R)h + \frac{2}{3}\phi_1(f+g)h' \\ &- \varepsilon(1-\phi)^{2.5}\delta(h')^2h'' + \frac{\phi_2 M^2\beta_e}{\beta_e^2+(1+\beta_e\beta_i)^2}R \\ &- \frac{\phi_2 M^2(1+\beta_e\beta_i)}{\beta_e^2+(1+\beta_e\beta_i)^2}h\Big]d\eta = 0,\end{aligned} \tag{21}$$

$$\begin{aligned}\int_{\eta_e}^{\eta_{e+1}} w_i\Big[&(1+\varepsilon(1-\phi)^{2.5})R'' - \frac{1}{3}\phi_1(h+R)R + \frac{2}{3}\phi_1(f+g)R' \\ &- \varepsilon(1-\phi)^{2.5}\delta(R')^2R'' - \frac{\phi_2 M^2\beta_e}{\beta_e^2+(1+\beta_e\beta_i)^2}h \\ &- \frac{\phi_2 M^2(1+\beta_e\beta_i)}{\beta_e^2+(1+\beta_e\beta_i)^2}h\Big]d\eta = 0,\end{aligned} \tag{22}$$

$$\begin{aligned}\int_{\eta_e}^{\eta_{e+1}} w_i\Big[&\Big(1+\frac{4}{3Nr}\Big)\theta'' + \frac{2k_f}{3k_{nf}}\phi_3\Pr(f+g)\theta' - \frac{2k_f}{3k_{nf}}\phi_3\Pr(h+R)\theta \\ &+ \frac{k_f}{k_{nf}}\frac{\phi_2}{(1-\phi)^{2.5}}\frac{M^2 Ec\Pr}{\beta_e^2+(1+\beta_e\beta_i)^2}(h^2+R^2)\Big]d\eta = 0,\end{aligned} \tag{23}$$

where $f' = h$, $g' = R$ and $w_i(i = 1, 2)$ are the weight functions.

Weak formulations of the said residual are given by

$$\begin{aligned}&\int_{\eta_e}^{\eta_{e+1}}\{-(1+\varepsilon(1-\phi)^{2.5})w'_ih' - \frac{1}{3}\phi_1(h+R)w_ih + \frac{2}{3}\phi_1(f+g)w_ih' + \varepsilon(1-\phi)^{2.5}\delta(h')^2w'_ih' + \tfrac{M^2\beta_e}{\beta_e^2+(1+\beta_e\beta_i)^2}w_i\phi_2R - \tfrac{M^2(1+\beta_e\beta_i)}{\beta_e^2+(1+\beta_e\beta_i)^2}w_i\phi_2h\}d\eta \\ &\quad = -\int_\Gamma((1+\varepsilon(1-\phi)^{2.5})w_ih' - \varepsilon(1-\phi)^{2.5}\delta(\overline{h}')^2w_ih')d\Gamma,\end{aligned}$$

$$\begin{aligned}&\int_{\eta_e}^{\eta_{e+1}}\{-(1+\varepsilon(1-\phi)^{2.5})w_iR' - \frac{1}{3}\phi_1(h+R)w_iR + \frac{2}{3}\phi_1(f+g)w_iR' + \varepsilon(1-\phi)^{2.5}\delta(R')^2w'_iR' - \tfrac{M^2\beta_e}{\beta_e^2+(1+\beta_e\beta_i)^2}w_i\phi_2h - \tfrac{M^2(1+\beta_e\beta_i)}{\beta_e^2+(1+\beta_e\beta_i)^2}w_i\phi_2h\}d\eta \\ &\quad = -\int_\Gamma((1+\varepsilon(1-\phi)^{2.5})w_iR' - \varepsilon(1-\phi)^{2.5}\delta(\overline{R}')^2w_iR')d\Gamma,\end{aligned}$$

$$\int_{\eta_e}^{\eta_{e+1}}[-(1+\tfrac{4}{3Nr})w'_i\theta' + \frac{2k_f}{3k_{nf}}\phi_3\Pr(f+g)w_i\theta' - \frac{2k_f}{3k_{nf}}\phi_3\Pr(h+R)w_i\theta + \tfrac{k_f}{k_{nf}}\tfrac{\phi_2}{(1-\phi)^{2.5}}\tfrac{M^2Ec\Pr}{\beta_e^2+(1+\beta_e\beta_i)^2}w_i(h^2+R^2)]d\eta = -\int_\Gamma(1+\tfrac{4}{3Nr})w_i\theta' d\Gamma,$$

where Γ is the boundary of the computational domain $[\eta_e, \eta_{e+1}]$.

Approximation of field variables: In FEM, the field variables are approximated over the typical line element $[\eta_e, \eta_{e+1}]$. The approximation of field variables is given by[32–35]

$$f = \sum_{j=1}^{2} f_j\psi_j, g = \sum_{j=1}^{2} g_j\psi_j, h = \sum_{j=1}^{2} h_j\psi_j, R = \sum_{j=1}^{2} R_j\psi_j \text{ and } \theta = \sum_{j=1}^{2}\theta_j\psi_j. \tag{24}$$

The unknown nodal values f_j, g_j, h_j, R_j and θ_j are to be computed. Using the above nodal approximations of the field variables in weak formulation of weighted residuals, one obtains the model of finite element of the form

$$[K^e\{\pi\}][\pi^e] = \{Q^e\} + \{F^e\},$$

where $[K^e\{\pi\}]$ is the stiffness matrix for typical element, π^e are unknown nodal values, $\{F^e\}$ is the boundary vector and $\{Q^e\}$ is the source vector. The stiffness and the boundary elements are given by

$$K_{ij}^{11} = \int_{\eta_e}^{\eta_{e+1}} \psi_i \frac{d\psi_j}{d\eta} d\eta, K_{ij}^{13} = -\int_{\eta_e}^{\eta_{e+1}} \psi_i\psi_j d\eta, K_{ij}^{12} = 0, K_{ij}^{14} = 0, K_{ij}^{15} = 0,$$

$$K_{ij}^{22} = \int_{\eta_e}^{\eta_{e+1}} \psi_i \frac{d\psi_j}{d\eta} d\eta, K_{ij}^{24} = -\int_{\eta_e}^{\eta_{e+1}} \psi_i\psi_j d\eta, K_{ij}^{21} = 0, K_{ij}^{23} = 0, K_{ij}^{25} = 0,$$

$$K_{ij}^{33} = \int_{\eta_e}^{\eta_{e+1}} [-(1+\varepsilon(1-\phi)^{2.5})\frac{d\psi_i}{d\eta}\frac{d\psi_j}{d\eta} + \frac{\varepsilon(1-\phi)^{2.5}\delta}{3}\frac{d\bar{h}}{d\eta}\frac{d\bar{h}}{d\eta}\frac{d\psi_i}{d\eta}\frac{d\psi_j}{d\eta} + \frac{2}{3}\phi_1(\bar{f}+\bar{g})\psi_i\frac{d\psi_j}{d\eta} - \frac{1}{3}\phi_1(\bar{h}+\bar{R})\psi_i\psi_j - \frac{M^2(1+\beta_e\beta_i)}{\beta_e^2+(1+\beta_e\beta_i)^2}\phi_2\psi_i\psi_j]d\eta,$$

$$K_{ij}^{34} = \int_{\eta_e}^{\eta_{e+1}} \frac{M^2\beta_e}{\beta_e^2+(1+\beta_e\beta_i)^2}\phi_2\psi_i\psi_j d\eta, K_{ij}^{31} = 0, K_{ij}^{32} = 0, K_{ij}^{35} = 0,$$

$$K_{ij}^{44} = \int_{\eta_e}^{\eta_{e+1}} [-(1+\varepsilon(1-\phi)^{2.5})\frac{d\psi_i}{d\eta}\frac{d\psi_j}{d\eta} + \frac{\varepsilon(1-\phi)^{2.5}\delta}{3}\frac{d\bar{R}}{d\eta}\frac{d\bar{R}}{d\eta}\frac{d\psi_i}{d\eta}\frac{d\psi_j}{d\eta} + \frac{2}{3}\phi_1(\bar{f}+\bar{g})\psi_i\frac{d\psi_j}{d\eta} - \frac{1}{3}\phi_1(\bar{h}+\bar{R})\psi_i\psi_j - \frac{M^2(1+\beta_e\beta_i)}{\beta_e^2+(1+\beta_e\beta_i)^2}\phi_2\psi_i\psi_j]d\eta,$$

$$K_{ij}^{43} = -\int_{\eta_e}^{\eta_{e+1}} \frac{M^2\beta_e}{\beta_e^2+(1+\beta_e\beta_i)^2}\phi_2\psi_i\psi_j d\eta, K_{ij}^{41} = 0, K_{ij}^{42} = 0, K_{ij}^{45} = 0, K_{ij}^{51} = 0, K_{ij}^{52} = 0, K_{ij}^{53} = 0,$$

$$K_{ij}^{53} = \int_{\eta_e}^{\eta_{e+1}} \frac{k_f}{k_{nf}}\frac{\phi_2}{(1-\phi)^{2.5}}\frac{M^2 Ec\Pr}{\beta_e^2+(1+\beta_e\beta_i)^2}\bar{h}\psi_i\psi_j d\eta, K_{ij}^{54} = \int_{\eta_e}^{\eta_{e+1}} \frac{k_f}{k_{nf}}\frac{\phi_2}{(1-\phi)^{2.5}}\frac{M^2 Ec\Pr}{\beta_e^2+(1+\beta_e\beta_i)^2}\bar{R}\psi_i\psi_j d\eta,$$

$$K_{ij}^{55} = \int_{\eta_e}^{\eta_{e+1}} [-(1+\frac{4}{3N_r})\frac{d\psi_i}{d\eta}\frac{d\psi_j}{d\eta} + \phi_3\frac{2k_f}{3k_{nf}}\Pr(\bar{f}+\bar{g})\psi_i\frac{d\psi_j}{d\eta} - \phi_3\frac{2k_f}{3k_{nf}}\Pr(\bar{h}+\bar{R})\psi_i\psi_j]d\eta,$$

and

$$b_{ij}^5 = \int_\Gamma -(1+\frac{4}{3Nr})\psi_i\frac{d\psi_j}{d\eta}d\Gamma, b_{ij}^4 = \int_\Gamma [\frac{\varepsilon(1-\phi)^{2.5}\delta}{3}\psi_i(\frac{d\psi_j}{d\eta})^3 - (1+\varepsilon(1-\phi)^{2.5})\psi_i\frac{d\psi_j}{d\eta}]d\Gamma,$$

$$b_{ij}^3 = \int_\Gamma [\frac{\varepsilon(1-\phi)^{2.5}\delta}{3}\psi_i(\frac{d\psi_j}{d\eta})^3 - (1+\varepsilon(1-\phi)^{2.5})\psi_i\frac{d\psi_j}{d\eta}]d\Gamma,$$

$$b_{ij}^2 = 0, b_{ij}^1 = 0,$$

respectively, where $\bar{f}, \bar{g}, \bar{h}$, and $\bar{R}$ are defined by

$$\bar{f} = \sum_{j=1}^{2}\bar{f}_j\psi_j, \bar{g} = \sum_{j=1}^{2}\bar{g}_j\psi_j, \bar{h} = \sum_{j=1}^{2}\bar{h}_j\psi_j, \bar{R} = \sum_{j=1}^{2}\bar{R}_j\psi_j,$$

The nodal values $\bar{f}_i$, $\bar{g}_i$, $\bar{h}_i$ and $\bar{R}_j$ are computed at the previous iteration. Detailed implementation of FEM to nonlinear fluid flow problems can be seen in References 32–35.

Assembly process: Elemental connectivity is used for the assembly process. By applying the above approximation to each element, one get the system of nonlinear algebraic equations of the form

$$[K\{\pi\}]\{\pi\} = \{F\}, \tag{25}$$

where $[K\{\pi\}]$ is global coefficient matrix whose element also involve unknown nodal values. An iterative procedure is adopt to solve the system of equations. This system is linearized by Picard's linearization method (see Refs. 32–35).

Programming: The system of algebraic equations is solved numerically by using Guass-Siedal approach. For computational procedure described above is implemented by using homemade cod programming. The developed computer code works with tolerance 10^{-5}. Computational experiments are done to search infinity for η. The asymptotic boundary conditions are satisfied when η is equal 12, *i.e.* [0,12] is the computational domain for the problem under consideration.

Error analysis and convergence: The error is formulated by using

$$error = |\pi^r - \pi^{r-1}|$$

and criteria for the convergence is set as

$$\max|\pi_i^r - \pi_i^{r-1}| < \xi$$

where ξ is the tolerance and it is taken equal to 10^{-5} in this analysis.

Grid independent study: Grid independent study is required when domain is discretize into small elements. The computed solutions are worthless if it depend on grid size. Therefore grid independent analysis is carried and obtain numerical values verses number of elements are tabulated in Table II. This table shows that f' and θ

TABLE II. Grid independent study for different number of grid sizes when $M = 0.9, \Pr = 3, \delta = 0.05, \varepsilon = 0.05, \beta_e = 1.2, \beta_i = 0.6, Ec = 2, N_r = 2$ and $\lambda = 0.5$ and $\phi = 0.05$.

No. of elements	$f'(\eta)$	$\theta(\eta)$
10	-1.012508	0.869378
50	-1.169453	0.997194
100	-1.174303	0.999152
150	-1.175077	0.999288
200	-1.175328	0.999302
250	-1.175439	0.999299
300	-1.175497	0.999295
350	-1.175533	0.999293
400	-1.175555	0.999289
450	-1.175570	0.999287
500	-1.175579	0.999283

are independent of grid size if the domain [0-12] is discretized into 500 elements.

IV. GRAPHICAL RESULTS AND THEIR DISCUSSION

Radivative heat transfer in three dimensional flow of partially ionized Erying-Powell liquid exposed to magnetic field is discussed and obtained results are displayed in Figures 2–36.

Behavior of velocity field: The behavior of different nanoparticles on the $x-$ component of velocity is shown by Fig. 2. This Fig. reflects that velocity f' for $\varphi = 0.15, 0.2$ (Al_2O_3- nanoparticles, TiO_2- nanopatticles) has highest values of velocity as compare to $\varphi = 0.05, 0.10$ ($Cu-$ nanoparticles, $Ag-$ nanopatticles). This shows that momentum for $\varphi = 0.15, 0.2$ diffuses (in $x-$ direction) faster than the diffusion of momentum (in $x-$ direction) for to $\varphi = 0.05, 0.10$. The influence of Hall force on the diffusion of wall momentum into Eyring-Powell liquid is displayed by Fig. 3.

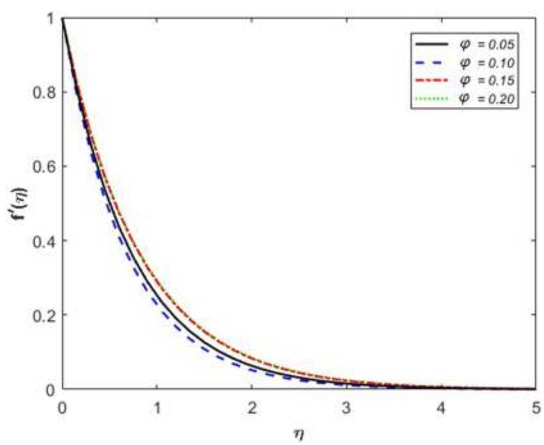

FIG. 2. Behavior of $f'(\eta)$ for various values of φ when $\varepsilon = 0.05, \delta = 0.05, M = 0.9, Ec = 2, \Pr = 3, N_r = 2, \beta_e = 1.2$ and $\beta_i = 0.6$.

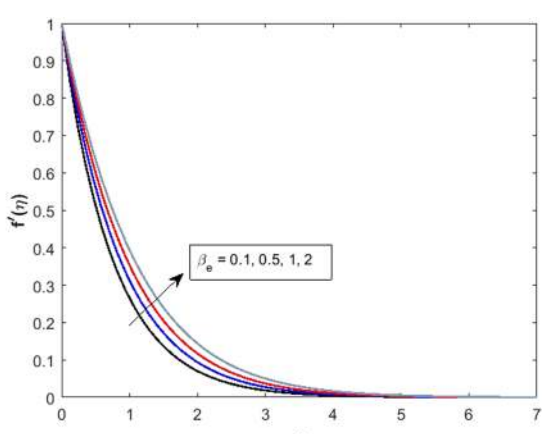

FIG. 3. Behavior of $f'(\eta)$ for various values of β_e on *Cu*-nano particles when $\varepsilon = 0.5, \delta = 0.8, M = 1.2, Ec = 2, \Pr = 3, N_r = 2$ and $\beta_i = 0.5$.

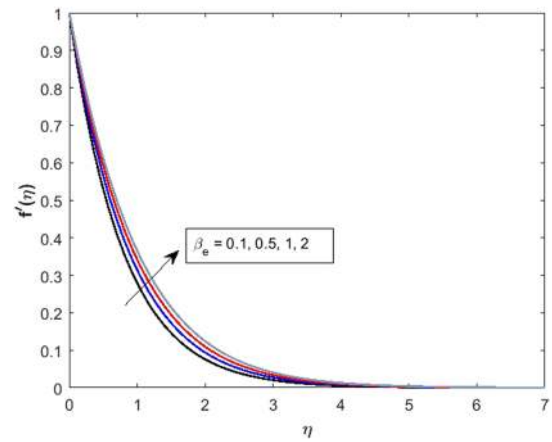

FIG. 4. Behavior of $f'(\eta)$ for various values of β_e on *Ag*-nano particles when $\varepsilon = 0.5, \delta = 0.8, M = 1.2, Ec = 2, \Pr = 3, N_r = 2$ and $\beta_i = 0.5$.

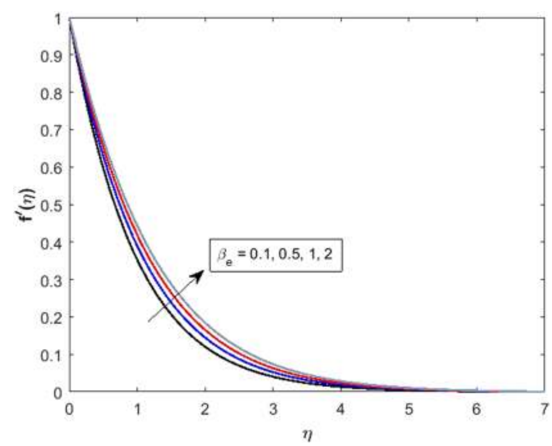

FIG. 5. Behavior of $f'(\eta)$ for various values of β_e on Al_2O_3- nano particles when $\varepsilon = 0.5, \delta = 0.8, M = 0.8, Ec = 2, \Pr = 3, N_r = 2$ and $\beta_i = 0.5$.

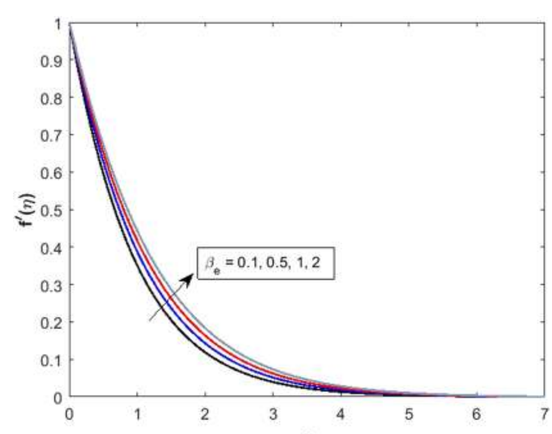

FIG. 6. Behavior of $f'(\eta)$ for various values of β_e on TiO_2-nano particles when $\varepsilon = 0.5, \delta = 0.8, M = 0.8, Ec = 2, \Pr = 3, N_r = 2$ and $\beta_i = 0.5$.

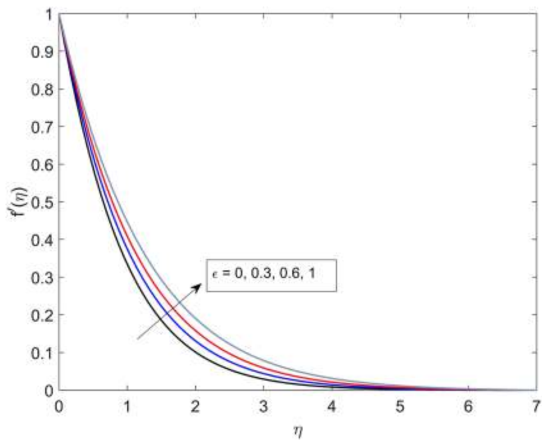

FIG. 7. Behavior of $f'(\eta)$ for various values of ε on *Cu*-nano particles when $\delta = 0.8, \beta_e = 1.2, M = 0.8, Ec = 3, \Pr = 3, N_r = 2$ and $\beta_i = 0.5$.

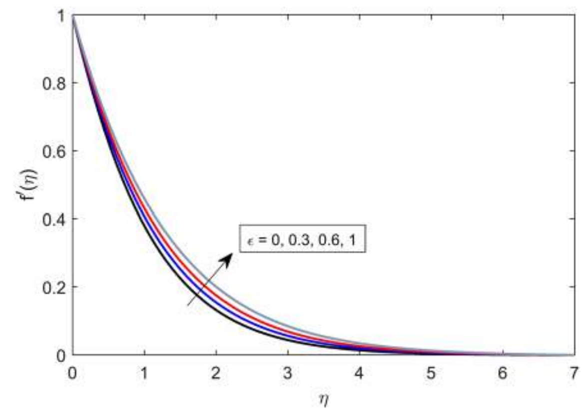

FIG. 10. Behavior of $f'(\eta)$ for various values of ε on *TiO$_2$*-nano particles when $\beta_e = 1.2, \delta = 0.8, M = 0.8, Ec = 3, \Pr = 3, N_r = 2$ and $\beta_i = 0.5$.

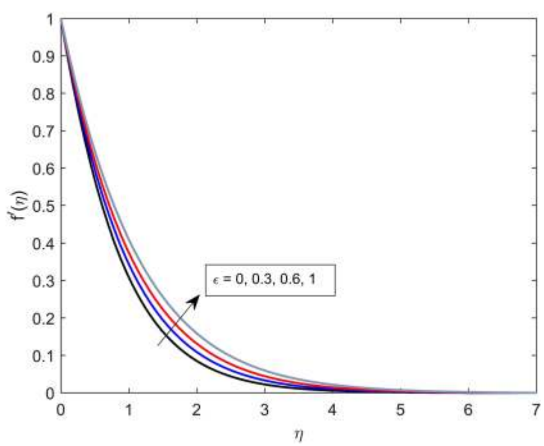

FIG. 8. Behavior of $f'(\eta)$ for various values of ε on *Ag*-nano particles when $\beta_e = 1.2, \delta = 0.8, M = 0.8, Ec = 3, \Pr = 3, N_r = 2$ and $\beta_i = 0.5$.

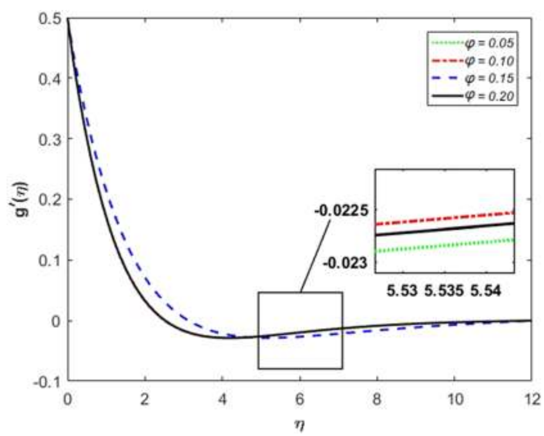

FIG. 11. Behavior of $g'(\eta)$ for various values of φ when $\varepsilon = 0.05, \delta = 0.05, M = 0.9, Ec = 2, \Pr = 3, N_r = 2, \beta_e = 1.2$ and $\beta_i = 0.6$.

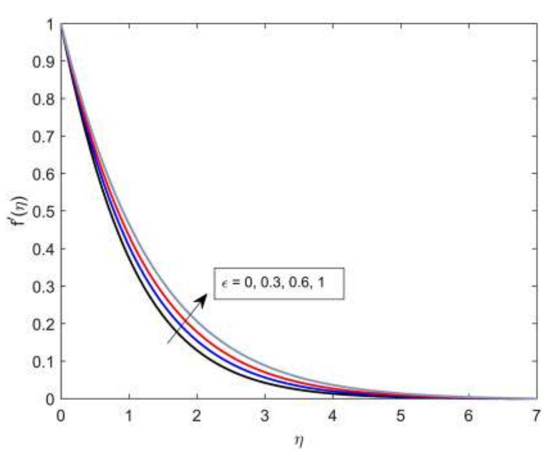

FIG. 9. Behavior of $f'(\eta)$ for various values of ε on *Al$_2$O$_3$*-nano particles when $\beta_e = 1.2, \delta = 0.8, M = 0.8, Ec = 3, \Pr = 3, N_r = 2$ and $\beta_i = 0.5$.

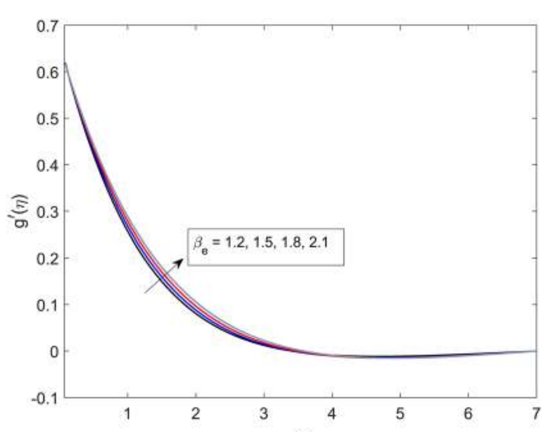

FIG. 12. Behavior of $g'(\eta)$ for various values of β_e on Cu-nanofluid when $\varepsilon = 0.5, \delta = 0.8, M = 1.2, Ec = 2, \Pr = 3, N_r = 2$ and $\beta_i = 0.6$.

This fig. depicts that velocity of Eyring-Powell liquid is in $x-$ direction is increased monotonically when Hall parameter β_e is increased. Similar trend is noted for $Ag-, Al_2O_3-$ and TiO_2- nanofluid and shown in Figs. 4–6.

The behavior of velocity under the variation of Eyring-Powell fluid parameter ε for the case of $Cu-, Ag-, Al_2O_3-$ and TiO_2- nanoparticles respectively shown by Figs. 7–10. It is found from these Figs. That the velocity of the fluid over a stretching sheet increases when Eyring-Powell fluid parameter ε is increased. It can also be concluded that the velocity of Newtonian liquid ($\varepsilon = 0$) is less than the velocity of Eyring-Powell liquid ($\varepsilon \neq 0$). A microscopic view in Fig. 11 explains about the $y-$ component of velocity profile in the presence of $Cu-, Ag-, Al_2O_3-$ and TiO_2- nano-particles. In the case of TiO_2 nano-particles $y-$ component of velocity is higher rather than the other nano-particles. It is perceived that boundary layer thickness of momentum is stronger when the $Cu-$ nano-particles are mixed into Erying-Powell plasma. Figs. 12–19 depict the effect of β_e, β_i and ε on the $y-$ component of velocity profile respectively.

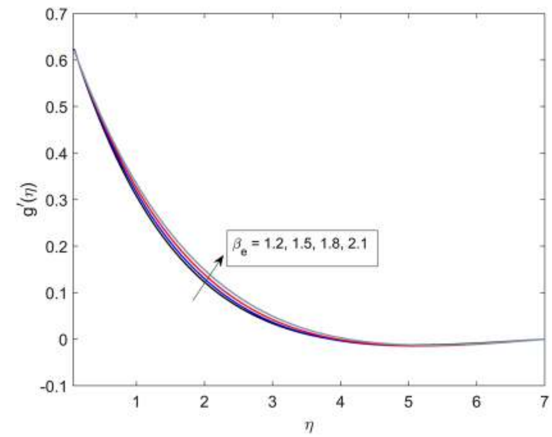

FIG. 15. Behavior of $g'(\eta)$ for various values of β_e on TiO_2-nano particles when $\varepsilon = 0.5, \delta = 0.8, M = 0.8, Ec = 2, \Pr = 3, N_r = 2$ and $\beta_i = 0.5$.

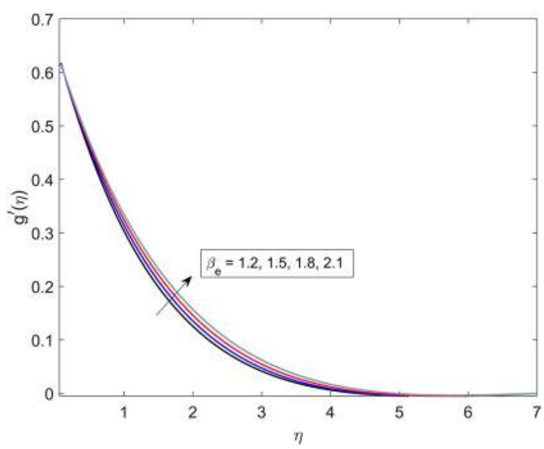

FIG. 13. Behavior of $g'(\eta)$ for various values of β_e on Ag-nanofluid when $\varepsilon = 0.5$, $\delta = 0.8, M = 1.2, Ec = 2, \Pr = 3, N_r = 2$ and $\beta_i = 0.6$.

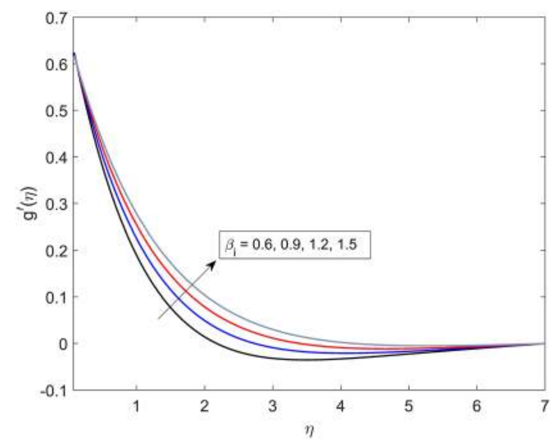

FIG. 16. Behavior of $g'(\eta)$ for various values of β_i on Cu-nano particles when $\varepsilon = 0.5, \delta = 0.8, M = 1.5, Ec = 3, \Pr = 3, N_r = 2$ and $\beta_e = 1.8$.

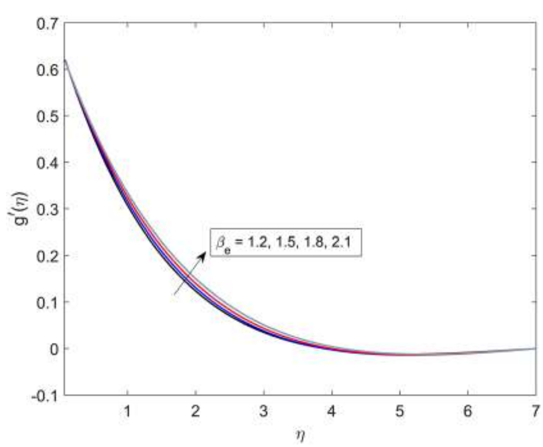

FIG. 14. Behavior of $g'(\eta)$ for various values of β_e on Al_2O_3-nano particles when $\varepsilon = 0.5, \delta = 0.8, M = 0.8, Ec = 2, \Pr = 3, N_r = 2$ and $\beta_i = 0.6$.

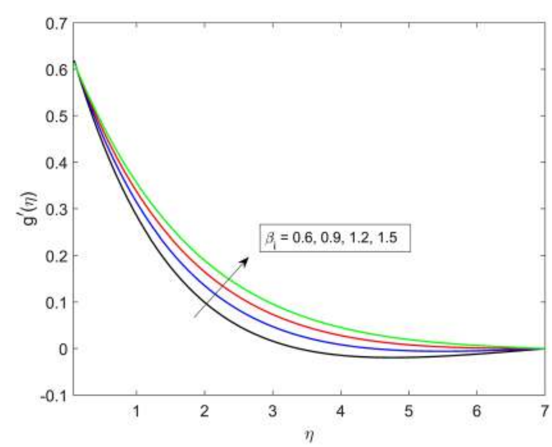

FIG. 17. Behavior of $g'(\eta)$ for various values of β_i on Ag-nano particles when $\varepsilon = 0.5, \delta = 0.8, M = 1.2, Ec = 3, \Pr = 3, N_r = 2$ and $\beta_e = 1.5$.

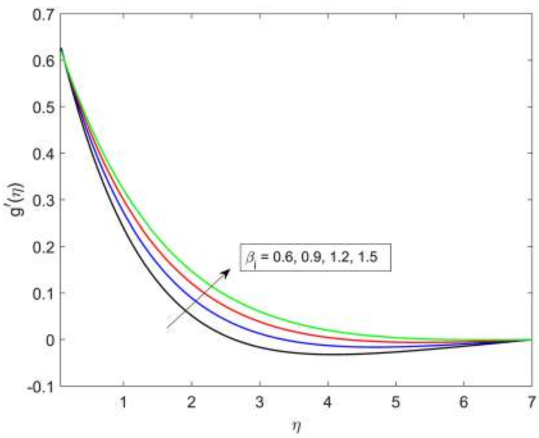

FIG. 18. Behavior of $g'(\eta)$ for various values of β_i on Al_2O_3-nano particles when $\varepsilon = 0.5, \delta = 0.8, M = 1.2, Ec = 3, \Pr = 3, N_r = 2$ and $\beta_e = 1.8$.

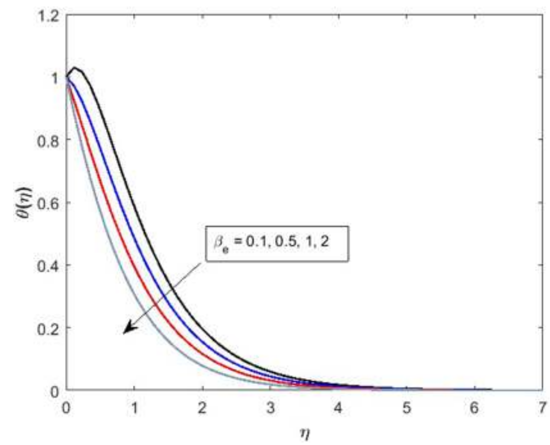

FIG. 21. Effect of β_e on temperature $\theta(\eta)$ in Cu-nanofluid when $\varepsilon = 0.5, \delta = 0.8, M = 1.2, Ec = 2, \Pr = 3, N_r = 2$ and $\beta_i = 0.5$.

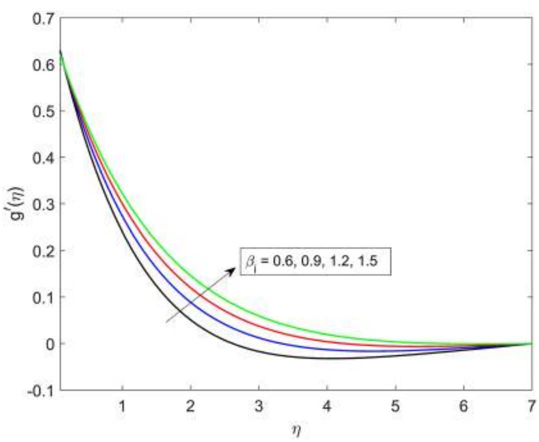

FIG. 19. Behavior of $g'(\eta)$ for various values of β_i on TiO_2-nano particles when $\varepsilon = 0.5, \delta = 0.8, M = 1.2, Ec = 3, \Pr = 3, N_r = 2$ and $\beta_e = 1.8$.

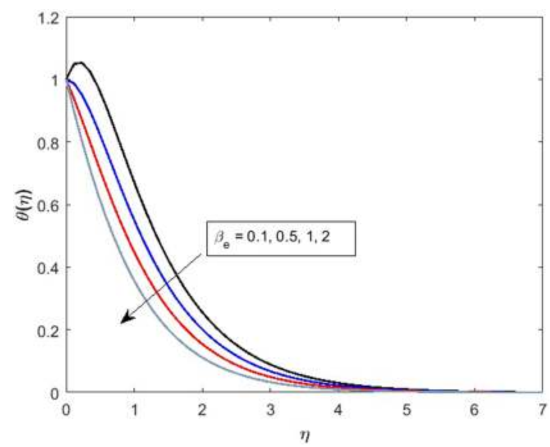

FIG. 22. Effect of β_e on temperature $\theta(\eta)$ in *Ag*- nanofluid when $\varepsilon = 0.5, \delta = 0.8, M = 1.2, Ec = 2, \Pr = 3, N_r = 2$ and $\beta_i = 0.5$.

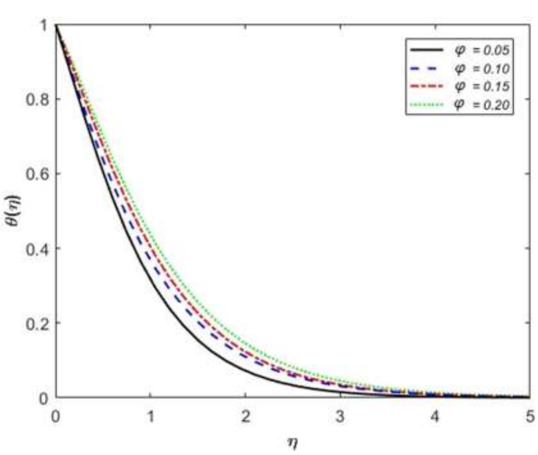

FIG. 20. Effect of ϕ on temperature $\theta(\eta)$ when $\varepsilon = 0.05, \delta = 0.05, M = 0.9, Ec = 2, \Pr = 3, N_r = 2, \beta_e = 1.2$ and $\beta_i = 0.6$.

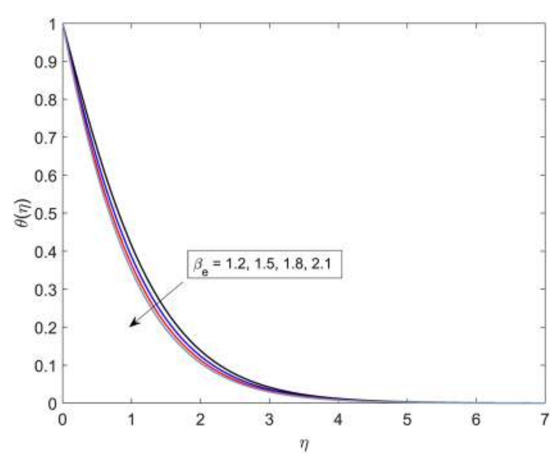

FIG. 23. Effect of β_e on temperature $\theta(\eta)$ in Al_2O_3- nanofluid when $\varepsilon = 0.5, \delta = 0.8, M = 0.8, Ec = 2, \Pr = 3, N_r = 2$ and $\beta_i = 0.5$.

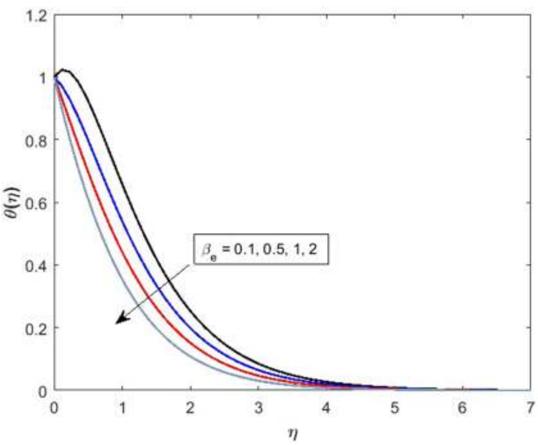

FIG. 24. Effect of β_e on temperature $\theta(\eta)$ in TiO_2- nanofluid when $\varepsilon = 0.5$, $\delta = 0.8$, $M = 0.8$, $Ec = 2$, $\Pr = 3$, $N_r = 2$ and $\beta_i = 0.5$.

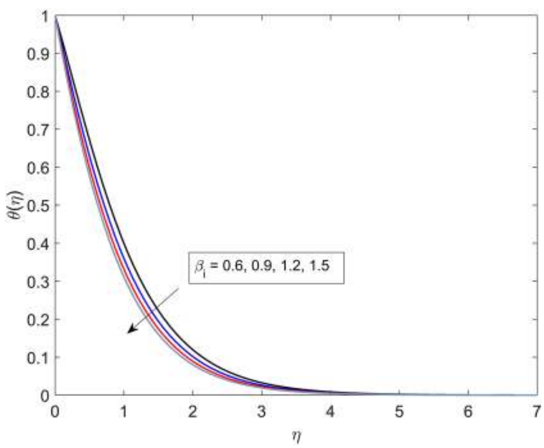

FIG. 25. Effect of β_i on temperature $\theta(\eta)$ in Cu- nanofluid when $\varepsilon = 0.5$, $\delta = 0.8$, $M = 1.5$, $Ec = 3$, $\Pr = 3$, $N_r = 2$ and $\beta_e = 1.8$.

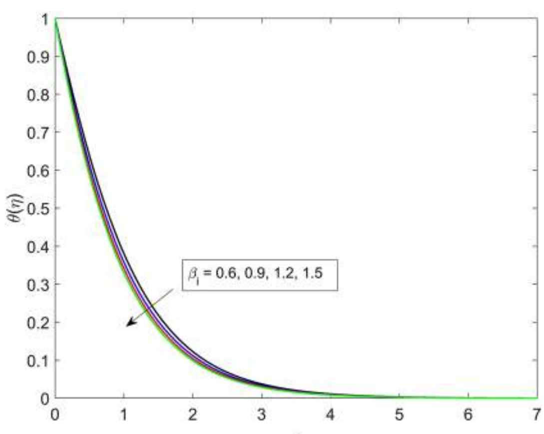

FIG. 26. Effect of β_i on temperature $\theta(\eta)$ in Ag- nanofluid when $\varepsilon = 0.5$, $\delta = 0.8$, $M = 1.2$, $Ec = 3$, $\Pr = 3$, $N_r = 2$ and $\beta_e = 1.5$.

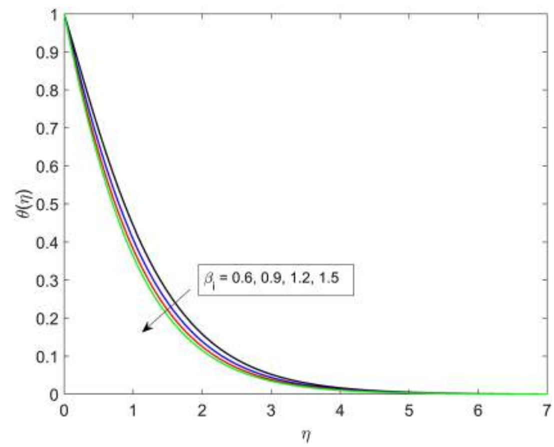

FIG. 27. Effect of β_i on temperature $\theta(\eta)$ in Al_2O_3- nanofluid when $\varepsilon = 0.5$, $\delta = 0.8$, $M = 1.2$, $Ec = 3$, $\Pr = 3$, $N_r = 2$ and $\beta_e = 1.8$.

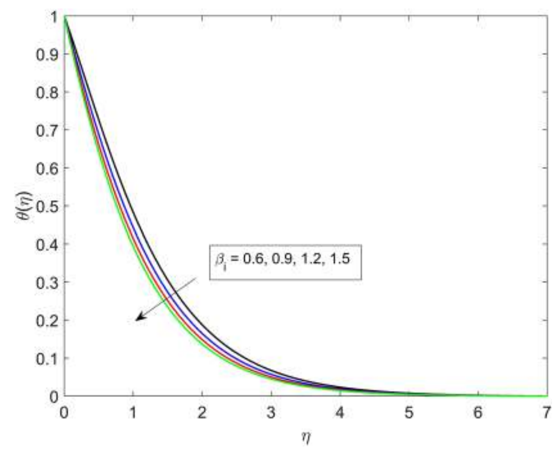

FIG. 28. Effect of β_i on temperature $\theta(\eta)$ in TiO_2- nanofluid when $\varepsilon = 0.5$, $\delta = 0.8$, $M = 1.2$, $Ec = 3$, $\Pr = 3$, $N_r = 2$ and $\beta_e = 1.8$.

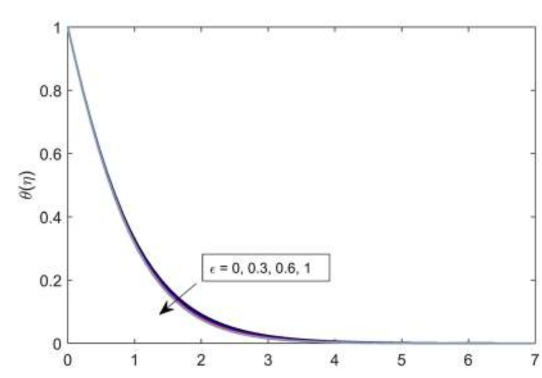

FIG. 29. Effect of ε on temperature $\theta(\eta)$ on cu- nanofluid when $\delta = 0.8$, $\beta_e = 1.2$, $M = 0.8$, $Ec = 3$, $\Pr = 3$, $N_r = 2$ and $\beta_i = 0.5$.

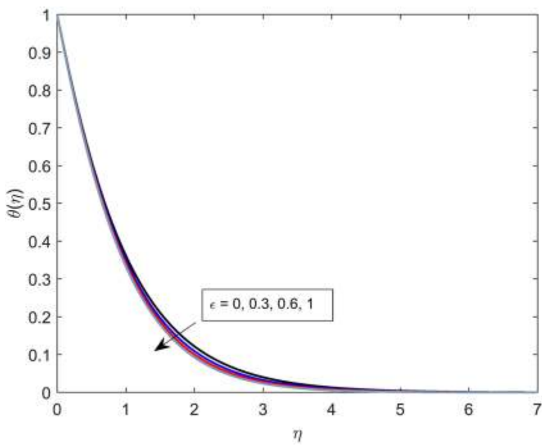

FIG. 30. Effect of ε on temperature $\theta(\eta)$ on *Ag*- nanofluid when $\delta = 0.8, \beta_e = 1.2$, $M = 0.8, Ec = 3$, Pr $= 3, N_r = 2$ and $\beta_i = 0.5$.

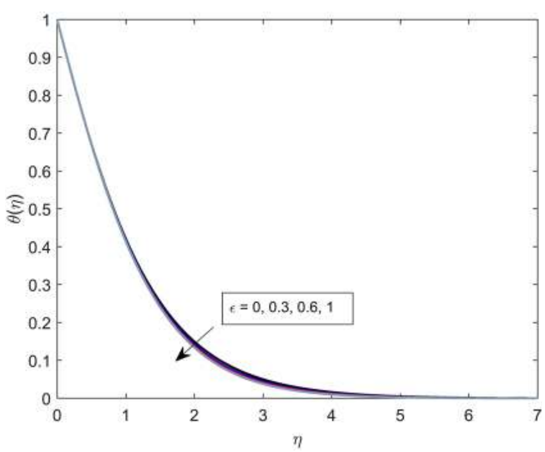

FIG. 31. Effect of ε on temperature $\theta(\eta)$ on *Al_2O_3*- nanofluid when $\delta = 0.8$, $\beta_e = 1.2, M = 0.8, Ec = 3$, Pr $= 3, N_r = 2$ and $\beta_i = 0.5$.

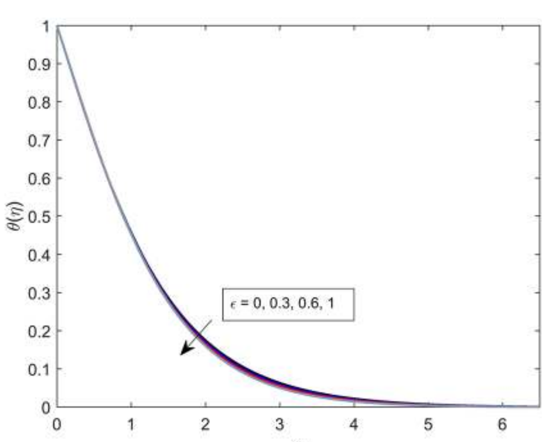

FIG. 32. Effect of ε on temperature $\theta(\eta)$ on *TiO_2*- nanofluid when $\delta = 0.8$, $\beta_e = 1.2, M = 0.8, Ec = 3$, Pr $= 3, N_r = 2$ and $\beta_i = 0.5$.

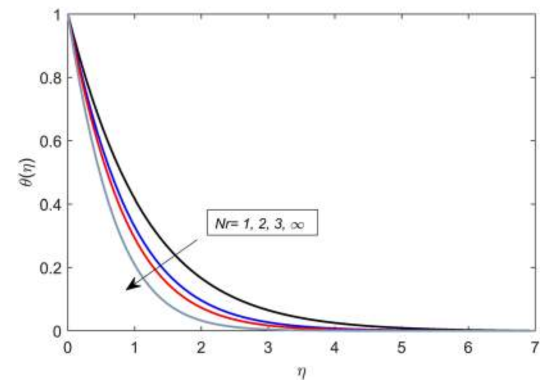

FIG. 33. Effect of β_i on temperature $\theta(\eta)$ in Cu- nanofluid $\delta = 0.05, M = 0.9$, $\varepsilon = 0.05, Ec = 2$, Pr $= 3, \beta_e = 1.2$ and $\beta_i = 0.6$.

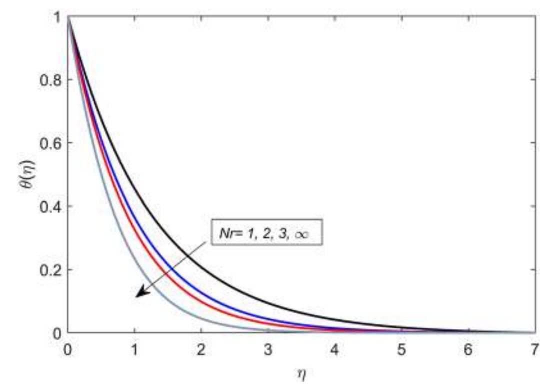

FIG. 34. Effect of β_i on temperature $\theta(\eta)$ in Ag– nanofluid $\delta = 0.05, M = 0.9$, $\varepsilon = 0.05, Ec = 2$, Pr $= 3, \beta_e = 1.2$ and $\beta_i = 0.6$.

Here it is noticed that the results of these parameters on $y-$ component of velocity are same as discussed in $x-$ component of velocity in Figs. 3–10. The expression $\beta_e^2 + (1 + \beta_e\beta_i)^2$ appear in the denominator of the components (x and y) of the Lorentz force. Therefore an increase in Hall and ion slip parameters (β_e and β_i) reduces the

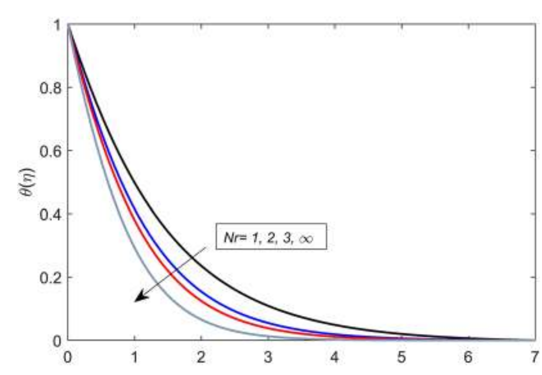

FIG. 35. Effect of Nr on temperature $\theta(\eta)$ in *Al_2O_3*– nanofluid $\delta = 0.05$, $M = 0.9, \varepsilon = 0.05, Ec = 2$, Pr $= 3, \beta_e = 1.2$ and $\beta_i = 0.6$.

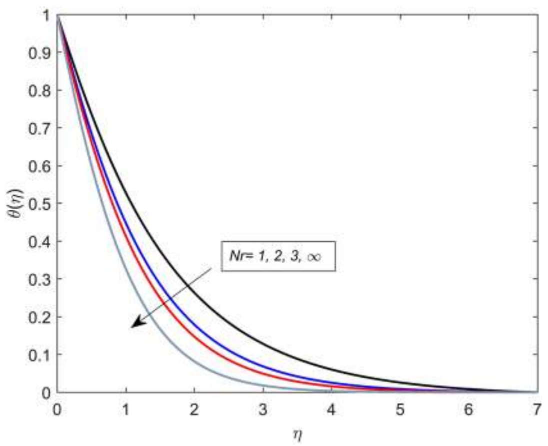

FIG. 36. Effect of Nr on temperature $\theta(\eta)$ in TiO_2- nanofluid $\delta = 0.05$, $M = 0.9, \varepsilon = 0.05, Ec = 2, \Pr = 3, \beta_e = 1.2$ and $\beta_i = 0.6$.

effect of Lorentz force. Consequently, flow in both x and y directions accelerates and Hall and ion slip currents are increased (see Figs 3–6 and 12–19).

Thermal changes in flow regime: The normalized temperature field for different nanoparticles Cu ($\varphi = 0.05$), Ag ($\varphi = 0.10$), Al_2O_3 ($\varphi = 0.15$) and TiO_2 ($\varphi = 0.20$) is displayed in Fig. 20. It is observed from Fig. 20 that temperature in mixture of TiO_2-nanoparticles and Eyring-Powell fluid is the highest as compare to the temperature of mixture of rest of $Cu-, Ag-, Al_2O_3-$ nanoparticles and Eyring-Powell liquid. Therefore, it is concluded that the wall temperature in mixture of Eyring-Poewll liquid and TiO_2-nanoparticles diffuses faster than that in mixture of Eyring-Poewll liquid and $Cu-, Ag-, Al_2O_3-$ nanoparticles. It is also noted that thermal boundary layer thickness in TiO_2- nanofluid is the highest as compare to the thermal boundary layer thickness associated with $Cu-, Ag-$ and Al_2O_3- nano-fluids see (Fig. 20). The temperature curves for nanoloquids verses variation of Hall parameter and ion slip parameter (β_e and β_i) are represented by Figs. 21–28. Figs. 21 and 25 depict that temperature of $Cu-$ nanofluid decreases when Hall parameter and ion slip parameter (β_e and β_i) are increased. This is due to the fact that β_e and β_i are appear in the denominator of Joule heating term and as denominator is increased, the coefficient of Joule heating term decreases. Consequently, the Joule heating effect is reduced and amount of heat due to Ohmic dissipation can be reduced by using partially ionized liquid exposed to magnetic field. The similar observation about the behavior of Hall parameter and ion slip parameter (β_e and β_i) on the temperature of $Ag-, Al_2O_3-$ and TiO_2- nanoparticles are noted (see Figs. 22–28). A significant behavior of fluid parameter ε on the temperature of nanofluid is noted and displayed by Fig. 29. It is found from Fig. 29 that the temperature of nanofluid decreases when fluid parameter ε is increased. It can also be noted from Fig. 29 that the temperature of Newtonian liquid ($\varepsilon = 0$) is greater than the temperature of Eyring-Powell liquid ($\varepsilon \neq 0$). Thermal boundary layer thickness of Newtonian liquid is greater than that for Eyring-Powell liquid. A similar trend is noted for $Ag-, Al_2O_3-$ and TiO_2- nanofluid (see Figs. 30–32).

TABLE III. Behavior of skin friction coefficient $(\mathrm{Re})^{1/2}C_{fx}$ for four types of nano-fluids when $M = 0.9$, $\Pr = 3, \delta = 0.05$, $\varepsilon = 0.05, \beta_e = 1.2$, $\beta_i = 0.6, Ec = 2, N_r = 2$ and $\lambda = 0.5$.

$$(\mathrm{Re})^{1/2}C_{fx} = -\left((1-\phi)^{-2.5}(1+\varepsilon)f''(0) - \tfrac{\varepsilon}{3}\delta(f''(0))^3\right)$$

		Cu	Ag	Al_2O_3	TiO_2
β_e	1.2	1.17346190	1.40766961	1.41984174	1.63798918
	1.5	1.14614909	1.38878503	1.37921335	1.59075360
	1.8	1.12684617	1.37575534	1.35016980	1.55697631
	2.2	1.10904546	1.36401457	1.32307237	1.52545139
β_i	0.6	1.17346190	1.40766961	1.41984174	1.63798918
	0.9	1.17374307	1.40952373	1.41872983	1.63663682
	1.2	1.17044683	1.40820722	1.41288551	1.62980434
	1.5	1.16563251	1.40545927	1.40512175	1.62075299
ε	0	1.14831935	1.37353659	1.37943514	1.58688173
	0.10	1.19859793	1.44157158	1.45964991	1.68828362
	0.20	1.24864058	1.50856135	1.53752020	1.78653799
	0.30	1.29813646	1.57433450	1.61315343	1.88184655

The effect of thermal radiation on the temperature of nanofluid (for the case of $Cu-, Ag-, Al_2O_3-$ and TiO_2 nano-particles) is shown by figures 33–36. The temperature of Erying-Powell fluid decreases when the intensity of thermal radiations is increased. This is due to the fact that fluid emits electromagnetic waves which carry the heat energy and consequently the fluid cools down. This observation is noted for all nanoparticles ($Cu-, Ag-, Al_2O_3-$ and TiO_2).

Normalized velocity and temperature gradients: Table III shows the comportment of $x-$ component of skin friction coefficient C_{f_x} for numerous values of ε, β_i and β_e It is perceived that $x-$component of skin friction coefficient of all nano-particles

TABLE IV. Behavior of skin friction coefficient $(\mathrm{Re})^{1/2}C_{gy}$ for four types of nano-fluids when $M = 0.9$, $\Pr = 3, \delta = 0.05, \varepsilon = 0.05\beta_e = 1.2, \beta_i = 0.6$, $Ec = 2, N_r = 2$ and $\lambda = 0.5$.

$$(\mathrm{Re})^{1/2}C_{gy} = -\left((1+\varepsilon)(1-\phi)^{-2.5}g''(0) - \tfrac{\varepsilon}{3}\delta(g''(0))^3\right)$$

		Cu	Ag	Al_2O_3	TiO_2
β_e	1.2	0.58297000	0.54507544	0.76927523	0.88881743
	1.5	0.55988474	0.52360289	0.73863056	0.85337596
	1.8	0.53747771	0.50277711	0.70888964	0.81898338
	2.2	0.50997175	0.47721269	0.67238565	0.77677404
β_i	0.6	0.58297000	0.54507544	0.76927523	0.88881743
	0.9	0.52192383	0.48846353	0.68825572	0.79513824
	1.2	0.47345426	0.44352892	0.62394188	0.72078313
	1.5	0.43441966	0.40735170	0.57215610	0.66091721
ε	0	0.56286900	0.52510235	0.74024370	0.85401682
	0.10	0.60265958	0.56466572	0.79783096	0.92311714
	0.20	0.64088827	0.60276500	0.85358488	0.99027561
	0.30	0.67770660	0.63952424	0.90763696	1.05561035

TABLE V. Behavior of Nusselt number when $M = 0.9, \Pr = 3, \delta = 0.05$, $\varepsilon = 0.05, \beta_e = 1.2, \beta_i = 0.6, Ec = 2, N_r = 2$ and $\lambda = 0.5$.

		$(\mathrm{Re})^{1/2}Nu = -\frac{k_{nf}}{k_f}\theta'(0)$			
		Cu	Ag	Al_2O_3	TiO_2
β_e	1.2	1.15602803	1.27075126	1.16570769	1.11596542
	1.5	1.23542760	1.33081842	1.28151732	1.25009862
	1.8	1.29139372	1.37274165	1.36352918	1.34501174
	2.2	1.34316196	1.41116768	1.43972242	1.43311070
β_i	0.6	1.15602803	1.27075126	1.16570769	1.11596542
	0.9	1.23309580	1.32818150	1.27918844	1.24758155
	1.2	1.28861208	1.36948864	1.36094333	1.34229274
	1.5	1.32940289	1.39977259	1.42105290	1.41185330
ε	0	1.15222713	1.26534971	1.16321473	1.11420763
	0.10	1.15948126	1.27579706	1.16798358	1.11756440
	0.20	1.16548820	1.28494253	1.17195617	1.12033266
	0.30	1.17049053	1.29299647	1.17525888	1.12259585

Cu, Ag, Al_2O_3 and TiO_2 is a decreasing function of β_e and β_i whilst it is mounting function of ε. The similar fashion is noted for $y-$ component of skin friction coefficient C_{g_y} (see Table IV). It is noted from the both tables the nano-particles of TiO_2 has the higher skin friction coefficient rather than Ag and Al_2O_3 nano-particles. Comportment of Nusselt number is displayed in Table V. It shows that the Nusselt number is mounting function of β_e, β_i and parameter ε for Cu, Ag, Al_2O_3 and TiO_2 nano-particles. It is perceived that the magnitude of Nusselt number in the case of Cu nano-particles achieves higher value than other nano-particles (Ag, Al_2O_3 and TiO_2).

V. CONCLUSION

The enhancement of heat transfer in Erying-Powell liquid in the presences of thermal radiation and Hall and ion-slip currents is studied via Galerkin finite element method (GFEM). Notable observations are listed below:

1. The distortion of magnetic lines by the fluid flow is responsible for Hall force which causes hindrance to the flow. This hindrance is reduced by the slip force. Therefore, a noteworthy increase in the velocity field is observed when the slip parameter is increased.
2. The momentum boundary layer thickness is greatly influenced by the dispersion of nanoparticles in the Erying-Powell liquid. The highest momentum boundary layer thickness is noted for the case of TiO_2- nano-particles.
3. Stresses at the surface of elastic wall have an increasing tendency when ion slip parameter is increased. Again force due to slip current is opposite to the force due to the applied magnetics field. Therefore, force per unit area decreases. Consequently, stresses have decreasing trend.
4. A significant rise in thermal conductivity due to the dispersion of four types of nanoparticles (Cu, Ag, Al_2O_3 and TiO_2) is noted. It is also observed that the dispersion of TiO_2 nanoparticles in Eyring-Powell liquid is responsible for the highest heat transfer as compare to the dispersion of Cu, Ag and Al_2O_3- nanoparticles in Eyring Powell liquids. Therefore, the dispersion of TiO_2 nanoparticles in Erying-Powell liquid is recommended if the maximum enhancement of heat transfer is required. The mixture of Erying-Powell liquid and Cu-nanoparticles is a good coolant in comparison of Ag, Al_2O_3 and TiO_2 nano particles.
5. The temperature of Erying-Powell liquid is an increasing function of the fluid parameter. The temperature of partially ionized Erying-Powell liquid is greater than the temperature of partially ionized Newtonian liquid. Thermal boundary layer thickness is in Erying-Powell liquid is greater than that in Newtonian liquid. However, Hall and ion slip currents in the Newtonian liquid play a significant role in reducing the temperature of the fluid. Consequently, thermal boundary layer thickness is decreased.
6. Wall heat flux increases when slip parameter is increased. However, it decreases when the fluid parameters is increased. Heat flux has for the case of TiO_2 nanoparticles has greater values than the values of Cu, Ag and Al_2O_3- nanoparticles

REFERENCES

[1] C. Srinivas Reddy, N. Kishan, and M. Madhu, "Finite element analysis of Erying-Powell nanofluid over an exponential stretching sheet," Int. J. Appl. Comput. Math. **4**, 8 (2018).

[2] S. Nadeem and S. Saleem, "Mixed convection flow of Erying-Powell fluid along a rotating cone," Results Phys. **4**, 54–62 (2014).

[3] T. Hayat, M. Awais, and M. Asghar, "Radiative effects in a three dimensional flow of MHD Eyying-Powell fluid," J. Egypt. Math. Soc. **21**(3), 379–384 (2013).

[4] M. M. Khader and A. M. Megahed, "Numerical studies for flow and heat transfer of the Powell-Erying fluid thin film over an unsteady stretching with internal heat generation using the Chebyshev finite difference method," J. Appl. Mech. Tech. Phys. **54**, 440–450 (2013).

[5] M. Jalil and S. Asghar, "Flow and heat transfer of Powell Erying fluid over a stretching surface, a Lie group analysis," J. Fluids Eng. ASME. **135**, 121–201 (2013).

[6] N. T. M. Elbade, S. N. Sallam, and M. Y. Abou-Zeid, "Numerical study of viscous dissipation effect on free convection heat and mass transfer of MHD non-Newtonian fluid flow through a porous medium," J. Egypt. Math. Soc. **20**, 139–151 (2012).

[7] M. Poonia and R. Bhargava, "Finite element study of Erying-Powell fluid flow with convective boundary conditions," J. Thermophys. Heat Transf. **28**, 3 (2014).

[8] T. Hayat, M. Farooq, A. Alsaedi, and Z. Iqbal, "Melting heat transfer in the stagnation point flow of Powell Erying fluid," J. Thermophys. Heat Transf. **27**(4), 761–766 (2013).

[9] T. Javed, N. ALi, Z. Abbas, and M. Sajjid, "Flow of an Erying-Powell non-Newtonian fluid over a stretching sheet," Chem. Eng. Commun. **200**(3), 327–336 (2013).

[10] N. A. Khan, S. Faqiha, and N. A. Khan, "Heat and mass transfer of thermophoretic MHD flow of Erying-Powell fluid over a vertical stretching sheet in the presence of chemical reaction and Joule heating," Int. J. Chem. React. Eng. **13**, 37–49 (2015).

[11] M. Ashraf Bilal, T. Hayat, and A. Alsaedi, "Three-dimensional flow of Erying-Powell nanofluid by convectively heated exponentially stretching sheet," Eur. Phys. J. Plus. **130**, 5 (2015).

[12] M. Bilal Ashraf, T. Hayat, S. A. Shehzad, and H. Malaikah, "Three-dimensional flow of viscoelastic fluid on an exponential stretching surface," Journal of Applied Mechanics and Technical Physics **57**(3), 446–456 (2016).

[13] M. Awais, T. Hayat, and A. Alsaedi, "Investigation of heat transfer in flow of Burger's fluid during a melting process," Journal of the Egyptian Mathematical Society **23**, 410–415 (2015).

[14] G. K. Ramesh, B. J. Gireesha, and C. S. Bagewadi, "MHD flow of a dusty fluid near the stagnation point over a permeable stretching sheet with non-uniform

source/sink," International Journal of Heat and Mass Transfer **55**, 4900–4907 (2012).
[15]M. Ramzan, M. Bila, and Jae Dong Chung, "Influence of homogeneous-heterogeneous reactions on MHD 3D Maxwell fluid flow with Cattaneo-Christov heat flux and convective boundary condition," Journal of Molecular Liquids **230**, 415–422 (2017).
[16]A. Majeed, A. Zeeshan, and R. Ellahi, "Chemical reaction and heat transfer on boundary layer Maxell Ferro-fluid flow under magnetic dipole with Soret and suction effects," Engineering Science and Technology an International Journal **20**, 1122–1128 (2017).
[17]S. Das, S. Chakaraborty, R. N. Jana, and O. D. Makinde, "Entropy analysis of unsteady magneto-nanofluid flow past accelerating stretching sheet with convective boundary condition," Appl. Math. Mech. -Engl. Ed. **36**, 1593–1610 (2015).
[18]T. Hayat, J. Akram, A. Alsaedi, and H. Zahir, "Endoscopy and homogeneous-heterogeneous reactions in MHD radiative peristaltic activity of Ree-Eyring fluid," Results Phys. **8**, 481–488 (2018).
[19]X. Chen, Y. Ye, X. Zhang, and L. Zheng, "Lie-group similarity solution and analysis for fractional viscoelastic MHD fluid over a stretching sheet," Comp. Math. Applic. **8**, 3002–3011 (2018).
[20]M. Turkyilmazoglu, "Analytical solutions to mixed convection MHD fluid flow induced by a nonlinearly deforming permeable surface," Commun. Nonlinear Sci. Numer. Simul. **63**, 373–379 (2018).
[21]S. Motsa and S. Shateyi, "The effects of chemical reaction, Hall and ion-slip currents on MHD micropolar fluid flow with thermal diffusivity using a novel numerical technical," J. App. Math. **9**, 1–30 (2012).
[22]T. Hayat, H. Zahir, A. Alsaedi, and B. Ahmad, "Hall current and Joule heating effects on peristaltic flow of viscous fluid in a rotating channel with convected boundary conditions," Results Phys, 2831–2836 (2017).
[23]T. Hayat and M. Nawaz, "Hall and ion-slip effects on three-dimensional flow of a second grade fluid," Int. J. Numer, Meth Fluids. **7**, 2831–2836 (2017).
[24]T. Hayat, A. Bibi, H. Yasmin, and B. Ahmad, "Simultaneous effects of Hall current and homogeneous/heterogeneous reactions on peristalsis," J. Taiwan Ins. Chem. Eng. **58**, 28–38 (2016).
[25]T. Hayat, M. Awais, M. Nawaz, S. Iram, and A. Saedi, "Mixed convection three-dimensional flow with Hall and ion-slip effects," Int. J. Nonlinear Sci. Number. Simul. **14**, 167–177 (2013).
[26]T. Hayat and M. Nawaz, "Soret and Dufour effects on the mixed convection flow of a second grade fluid subject to Hall and ion-slip current," Int. J. Num. Methods fluids **66**, 1073–1099 (2011).
[27]T. Hayat, M. Shafique, A. Tanveer, and A. Alsaedi, "Hall and ion slip effects on peristaltic flow of Jeffery nanofluid with Joule heating," J. Mag, Mag. Mat. **407**, 51–59 (2016).
[28]M. Nawaz, T. Hayat, and A. Alsaedi, "Mixed convection three-dimensional Maxwell fluid flow in the presence of Hall and ion-slip effects," J. Heat Trans. **135**, 1–8 (2013).
[29]T. Hayat, A. Shafiq, and A. Alseadi, "Effect of joule heating and thermal radiation in the flow of third grade fluid over radiative surface," PLOS One **9**(1), 1–12 (2014).
[30]T. Hayat, M. Awais, A. Alsaedi, and A. Safdar, "On computations for thermal radition in MHD channel flow with heat and mass transfer," PLOS One **9**(1), 1371–1383 (2014).
[31]T. Hayat and M. Qasim, "Radiation and mass transfer effects on the magnetohydrodynamic unsteady mixed convection flow of second grade fluid over a vertical stretching sheet," Int. J. Num. Meth. Fluid. **66**, 820–832 (2011).
[32]M. Nawaz and T. Zubair, "Finite element study of three dimensional radiative nano-plasma flow subject to Hall and ion slip currents," Results Phys **7**, 4111–4122 (2017).
[33]I. H. Qureshi, M. Nawaz, S. Rana, and T. Hayat, "Galerkin finite element study on the effects of variable thermal conductivity and variable mass diffusion conductance on heat and mass transfer," Commun. Theor. Phys. **70**, 49–59 (2018).
[34]I. H. Qureshi, M. Nawaz, S. Rana, Umar Nazir, and A. J. Chamkha, "Investigation of variable thermo-physical properties of viscoelastic rheology: A Galerkin finite element approach," AIP Advances **8**(7), 075027-1–075027-16 (2018).
[35]M. Nawaz, S. Rana, I. H. Qureshi, and T. Hayat, "Three-dimensional heat transfer in the mixture of nanoparticles and micropolar MHD plasma with Hall and ion slip effects," AIP Advances **8**, 105109 (2018).